Chromosome biorientation and APC activity remain uncoupled in oocytes with reduced volume

Simon I.R. Lane[1,2] and Keith T. Jones[1,2]

[1]Biological Sciences, Faculty of Natural and Environmental Sciences, University of Southampton, Southampton, UK
[2]School of Biomedical Sciences and Pharmacy, University of Newcastle, Callaghan, New South Wales, Australia

The spindle assembly checkpoint (SAC) prevents chromosome missegregation by coupling anaphase onset with correct chromosome attachment and tension to microtubules. It does this by generating a diffusible signal from free kinetochores into the cytoplasm, inhibiting the anaphase-promoting complex (APC). The volume in which this signal remains effective is unknown. This raises the possibility that cell volume may be the reason the SAC is weak, and chromosome segregation error-prone, in mammalian oocytes. Here, by a process of serial bisection, we analyzed the influence of oocyte volume on the ability of the SAC to inhibit bivalent segregation in meiosis I. We were able to generate oocytes with cytoplasmic volumes reduced by 86% and observed changes in APC activity consistent with increased SAC control. However, bivalent biorientation remained uncoupled from APC activity, leading to error-prone chromosome segregation. We conclude that volume is one factor contributing to SAC weakness in oocytes. However, additional factors likely uncouple chromosome biorientation with APC activity.

Introduction

To be effective against chromosome missegregation, the spindle assembly checkpoint (SAC) must prevent anaphase until all chromosomes are correctly attached to spindle microtubules, a state called biorientation (Foley and Kapoor, 2013; Musacchio, 2015). It does this by using free kinetochores as a platform for generating a diffusible inhibitor of the anaphase-promoting complex (APC), a cytoplasmic mitotic checkpoint complex (Jia et al., 2013; Pesenti et al., 2016). One would imagine that, in a robust checkpoint such as that exhibited by somatic cells, the inhibitory signal would prevent APC activity throughout the entire cytoplasm. However, there may be a limit on how far the signal can diffuse before it becomes too dilute to be effective. Previous work in PtK1 cells has shown the inability of a non-bioriented chromosome on one spindle to influence anaphase onset on an adjacent spindle in a shared cytoplasm (Rieder et al., 1997), raising the possibility of a limit on the effective distance of the inhibitory signal. More recent studies in fused cells show that the strength of the SAC is also diminished by both diffusion barriers and dilution by nonmitotic cytoplasm (Heasley et al., 2017).

Oocytes are much larger than somatic cells, raising the question of how the SAC can regulate the APC within this much larger volume. It is possible that in such large cells the SAC cannot fully inhibit APC activity. Indeed, in *Xenopus laevis* eggs, which are ∼1 mm in diameter, there does not appear to be any influence of the SAC on meiotic divisions (Shao et al., 2013; Liu et al., 2014). However, SAC activity can be restored by raising the nuclear:cytoplasmic ratio by adding sperm nuclei to cytoplasmic *Xenopus* egg homogenates (Minshull et al., 1994). Furthermore, in the developing embryos of several species including *Xenopus*, *Caenorhabditis elegans*, and zebrafish, there is considerable interest in cell size and developmental timers on the establishment of the SAC during embryogenesis (Clute and Masui, 1995; Zhang et al., 2015; Galli and Morgan, 2016).

Mammalian oocytes are typically 70–150 µm in diameter, depending on species, and are large enough to present a volume in which the predicted reach of the SAC is exceeded. In contrast to *Xenopus*, the SAC is certainly physiologically active during the meiotic divisions of mammalian oocytes, and as such, knockdown/knockout of any one component of the checkpoint raises aneuploidy rates (Homer et al., 2005; McGuinness et al., 2009; Hached et al., 2011). However, it is generally regarded that the SAC is weak in its surveillance of misalignment or nonattachment because it cannot prevent anaphase when a small number of bivalents are not bioriented in mouse oocytes (Nagaoka et al., 2011; Gui and Homer, 2012; Kolano et al., 2012; Lane et al., 2012; Sebestova et al., 2012). Such loss of APC control by a weak SAC would account for the higher rates of aneuploidy observed in oocytes during their first meiotic division (meiosis I [MI]; Jones and Lane, 2013; Merriman et al., 2013; Gorbsky, 2015; Touati and Wassmann, 2016). Indeed, control of APC by the SAC appears weak enough that during the major part of MI,

Correspondence to Simon I.R. Lane: simon.lane@soton.ac.uk

Abbreviations used: APC, anaphase promoting complex; CenpC, centromere protein C; cRNA, complementary RNA; H2B, Histone 2B; MI, meiosis I; NEB, nuclear envelope breakdown; PBE, polar body extrusion; SAC, spindle assembly checkpoint.

The Rockefeller University Press
J. Cell Biol. Vol. 216 No. 12 3949–3957
https://doi.org/10.1083/jcb.201606134

when the APC is at its greatest measureable activity, the SAC is still partially on (Lane and Jones, 2014). All these observations collectively point to mammalian oocyte size being an important factor that limits the ability of the SAC to inhibit the APC.

Recently, it has been shown that a reduction in the size of mouse oocytes by half enforces the SAC, if the volume reduction occurs before nuclear envelope breakdown (NEB; Kyogoku and Kitajima, 2017). However, the reduction in oocyte volume also occurs with a concentration of SAC components being formed at the nuclear envelope. Here, we set out to test the strength of the SAC generated by the (pro)metaphase kinetochores, without the confounding effects of enriching SAC components, by using a procedure of repeatedly bisecting oocytes after NEB to achieve a highly miniaturized cell with a volume reduced by ∼86%. We found that the spindle scales in proportion to the cytoplasmic volume, and the timing of APC activation is delayed; however, it still remains uncoupled from the normal process of bivalent biorientation. Subsequent use of low doses of spindle poison in a reduced volume decreases bivalent biorientation success and activates the SAC to a greater extent than in large oocytes. We demonstrate that the volume limit at which the SAC signal from individual bivalents might be effective is far less than ∼one-eighth that of a normal mouse oocyte (<27 pL).

Results and discussion

To examine the influence that cell volume has on the ability of the SAC to arrest mouse oocytes in MI, we first set about producing oocytes of varying sizes. We established a serial bisection technique using cytochalasin D, which has been used previously for halving oocytes in a single procedure (Hoffmann et al., 2011; Polanski and Kubiak, 2013). Immediately after NEB, oocytes could be bisected up to three times, and we defined these products as B_1, B_2, and B_3 oocytes (bisected once, bisected twice, or bisected three times), which created cells of one half, one quarter, and one eighth their original volume, respectively (Fig. 1 A). We also produced serially sham-bisected oocytes (B_0), in which the bisection procedure was aborted just before cleaving the oocyte in two. The two halves were still connected by a thin cytoplasmic bridge and reformed a single spherical shape within 1–2 min. The bisection procedure was reproducibly accurate, with serially bisected oocytes having volumes of 190 ± 17 (B_0), 93 ± 15 (B_1), 50 ± 11 (B_2), and 27 ± 6 pL (B_3) and radii of 36 ± 1 (B_0), 28 ± 1 (B_1), 23 ± 2 (B_2), and 18 ± 1 µm (B_3; Fig. 1, B and C). Chromosome counts demonstrated that 95% (n = 20) of B_3 oocytes contained the correct number of 20 bivalents after triple bisection, showing that the chromosomes had not been dispersed during the procedure (Fig. S1, A and B).

To verify that the oocytes' reduced volume did not affect their ability to form a spindle, we microinjected complementary RNA (cRNA) for histone 2B (H2B)–mCherry and β-tubulin-GFP. Oocytes were examined 7 h after NEB, a time when spindles are fully formed (Schuh and Ellenberg, 2007). We observed normal anastral barrel-shaped spindle morphology independent of volume (Fig. 1 D). Overall, both spindle pole-to-pole length and equatorial width declined as oocytes became smaller (Fig. S1 C), such that the ratio of spindle volume to oocyte volume remained relatively constant (Fig. S1 D). Therefore, spindles of mammalian oocytes demonstrate the same ability to scale in proportion to cell size as do *Xenopus* eggs (Good et al., 2013; Hazel et al., 2013). Importantly, the serial bisection procedure had no impact on the ability of oocytes to complete MI, with 60–70% demonstrating polar body extrusion (PBE) independently of size (Fig. 1 E).

In summary, we have established a procedure that can reduce the volume of an oocyte eightfold. The resulting volume is still larger than that of a somatic cell (27 pL here vs. ∼0.1–10 pL for various mammalian cells). However, the reduced volume of the B_3 cell raises the possibility that the SAC signal may be able to penetrate the cytoplasm at sufficient concentration to increase the efficacy of the SAC.

To investigate whether reducing oocyte volume had changed the properties of the SAC, we measured the degradation of the APC substrate securin (Herbert et al., 2003; Holt et al., 2013). Securin degradation gives a real-time measure of APC activity, a process in oocytes that is not dependent on the presence of bivalents after serial bisection (Fig. 2 A). Such a finding is in agreement with previous studies on oocytes after a single bisection procedure (Hoffmann et al., 2011; Lane and Jones, 2014) and demonstrates that active APC is dispersed throughout the oocyte cytoplasm.

B_0 and B_3 oocytes expressing securin-YFP and H2B-mCherry, and containing bivalents, were imaged by time-lapse microscopy to record securin loss and monitor bivalent segregation at anaphase (Fig. 2 B). For each oocyte, the times of NEB and anaphase were recorded, as well as the point at which securin degradation was initiated between the two events. The initiation of securin loss we term "APC activation." B_3 oocytes spent significantly more time in MI (measured as the interval between NEB and anaphase) compared with B_0 (B_3, 9.8 ± 1.8 h; B_0, 9.0 ± 1.3 h; P = 0.0234; Fig. 2 C). However, more striking differences were observed when the period between NEB and APC activation was measured, as well as the period between APC activation and anaphase (Fig. 2 D). Comparison of these timings in B_0 and B_3 oocytes revealed that securin remained stable significantly longer in the B_3 oocytes (B_0, 6.6 ± 0.9 h; B_3, 7.9 ± 1.7 h; P < 0.0001), but was then degraded in a significantly shorter time (B_0, 2.4 ± 0.7 h; B_3, 1.8 ± 0.4 h; P = 0.0002). Consistent with this, we found that in percentage terms, the peak APC activity was significantly greater in the B_3 oocytes (B_0, 48.9 ± 9.15% per h; B_3, 62.1 ± 22.5% per h; P = 0.0007; Fig. 2, E and F).

These observations suggest that APC regulation was subtly changed in a reduced oocyte volume, such that there was a longer period of prometaphase, in which the APC is not active, but then a shorter metaphase–anaphase transition, caused by increased APC activity. This is somewhat reminiscent of the more switch-like transition in APC activity seen in mitotic cells (Clute and Pines, 1999), and it is a finding that would be consistent with the SAC having greater control over the APC during prometaphase, before the APC is active. However, many other interpretations are possible for why the periods of NEB-APC activation and APC activation-anaphase differ. For example, there may have been changes in the ability to assemble a smaller, more crowded, spindle in B_3 oocytes, or differences in the segregation of any protein between nucleoplast and cytoplast, which may have affected the timing of meiosis.

We decided to test whether the change in the timing of APC activation during MI in B_3 oocytes was because the SAC was more effective in inhibiting the APC in the presence of non-bioriented bivalents. If so, one would expect to observe only bioriented bivalents during the 2–3 h of APC activity preceding

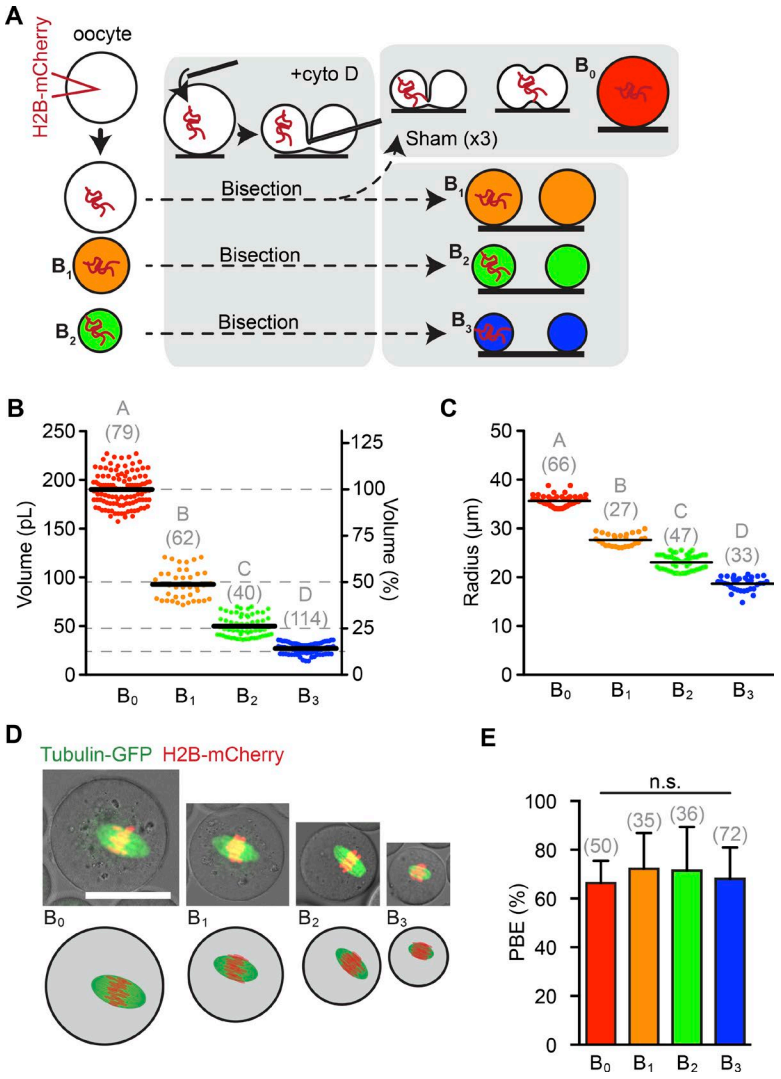

Figure 1. **Repeated oocyte bisection produces small oocytes that undergo MI.** (A) Schematic of the triple bisection procedure showing the generation of B_0, B_1, B_2, and B_3 oocytes. The same colors are adopted for all figures throughout. (B) Oocyte volumes expressed in pL (left axis) or as a percentage of full size oocytes (right axis). Dashed horizontal lines show the expected sizes of half, quarter, and eighth oocytes. (C) Oocyte radii after bisection. (D) Representative images of oocytes expressing tubulin-GFP and H2B-mCherry, with cartoon depiction underneath. Bar, 50 µm. (E) Percentage of oocytes completing MI; n.s. not significant. Error bars indicate 95% confidence interval. In B, C, and E, numbers of oocytes used are indicated in parentheses. In B and C, groups without common letters indicate significant differences (analysis of variance with Tukey's correction for multiple comparisons; $P < 0.0001$).

anaphase (Fig. 2 E). However, four-dimensional confocal scanning laser microscopy imaging of live oocytes expressing H2B-mCherry and centromere protein C (CenpC)–GFP at that time revealed several examples of bivalents moving on and off the spindle equator, showing them to be in the process of establishing biorientation (Fig. 3 A, arrowheads; and Video 1). Three objective measurements of biorientation in live oocytes were made (Fig. 3 B): bivalent stretch (distance between the kinetochore pairs), displacement (from the metaphase plate), and θ (angle bivalent intersects the metaphase plate). For each bivalent, these measures were compared against those of fully bioriented control oocytes matured to metaphase (8 h after NEB; Collins et al., 2015). Bivalents >3 SDs away from the mean control values in any of the three measures were considered non-bioriented. Using this analysis, we observed non-bioriented bivalents in live oocytes during the 2–3 h before anaphase (Fig. 3 C), and even in the minutes immediately before anaphase (Fig. 3, C and D; and Video 1). In addition, we found no significant differences between B_0 and B_3 oocytes at any of the time points assessed in terms of the number of non-bioriented bivalents per oocyte (Fig. 3, C, E, and F), suggesting that the reduced volume was not significantly affecting the ability of bivalents to biorient.

The presence of non-bioriented bivalents during the period of APC activity in B_3 oocytes suggests that reducing oocyte volume had not had any beneficial effect on the ability of the SAC to inhibit the APC in response to a small number of attachment errors. We were not technically able to bisect B_3 oocytes further to determine if reducing the oocyte volume <27 pL had any greater impact on the dynamics of APC activity. However, we could increase the number of bivalents not bioriented using a low dose of the spindle poison nocodazole, which does not block anaphase in fully sized oocytes (Collins et al., 2015). We wondered whether an increased number of non-bioriented chromosomes in conjunction with a reduced oocyte volume would provide a situation in which the SAC could restrain the APC.

B_3 and B_0 oocytes were cultured in 0 or 25 nM nocodazole throughout MI and scored for PBE. Nocodazole at this dose caused a significant decrease in PBE for B_3 but not for B_0 oocytes (B_3, 34/50 vs. 15/39, $P = 0.0095$; B_0, 69/104 vs. 65/90, $P = 0.7647$; Fig. 4 A). We reasoned that B_3 oocytes could be more sensitive to nocodazole, either because of an increased SAC efficiency or because the nocodazole had a greater ability to disrupt bivalent biorientation in B_3 than in B_0 oocytes. Upon examination of the bivalents we favored the latter explanation, as non-bioriented bivalents were always observed at a greater frequency in the B_3 oocytes: in the 2 h preceding anaphase, B_0 oocytes had 0–4 (mean 1.6), whereas B_3 oocytes had 3–12 (mean 5.4; Fig. 4, B and C; and Video 2). The ability of

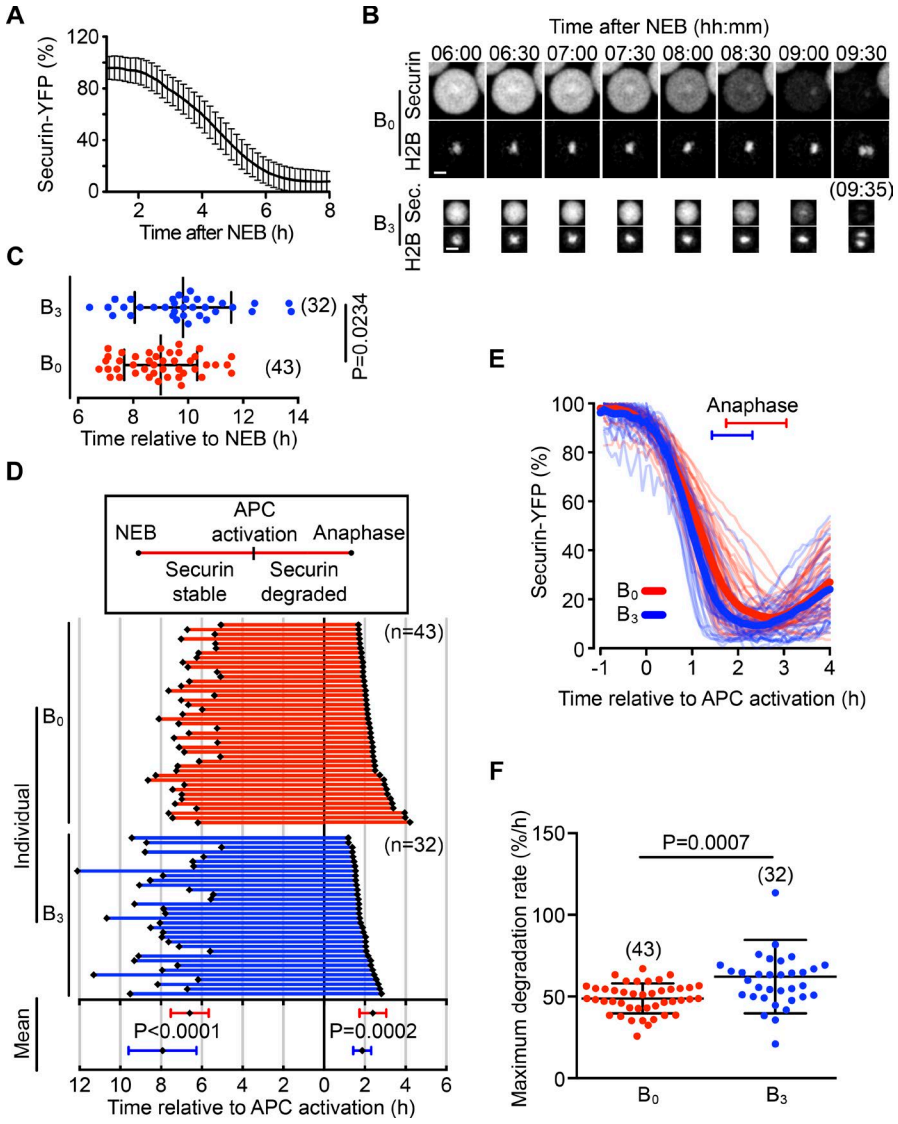

Figure 2. **Smaller oocytes spend longer in prometaphase but then have a faster rate of securin loss.** (A) Relative securin degradation traces from B_3 cytoplasts lacking chromosomes after bisection. (B) Representative time lapse of B_0 (top) and B_3 (bottom) oocytes expressing securin-YFP and H2B-mCherry relative to time after NEB. Bar, 10 µm. (C) Timing of anaphase relative to NEB, determined from images as in B. There is no significant difference in the time of anaphase between B_0 and B_3 oocytes. (D) Timing of NEB (left) and anaphase (right) relative to activation of the APC. Plots for individual oocytes are displayed above, with means below. (E) Individual (pale) and mean (bold) securin traces from B_0 and B_3 oocytes, arranged relative to the time of APC activation. Horizontal bars show the corresponding timing of anaphase. (F) Maximal rate of securin destruction recorded from traces as in E. In C, D, and F, numbers of oocytes used are indicated in parentheses. In C, D, and F, statistical test was unpaired *t* test. Error bars indicate SD.

nocodazole to have a greater disruptive influence on the spindle of B_3 oocytes may be because the drug penetration is greater in a smaller volume (there is a two times greater surface area :volume ratio in a B_3 oocyte vs. a B_0 oocyte), or a greater ability to impact on a smaller and more crowded spindle (Fig. 1 D). As such, in B_3 oocytes, 29% of the bivalents were classified as non-bioriented. Furthermore, 5 min before anaphase, 25% of bivalents remained non-bioriented (Fig. 4, D and E), demonstrating that these chromosomes persistently failed to attach correctly to the spindle.

We next sought to adjust the nocodazole concentration such that both B_0 and B_3 oocytes experienced very similar levels of bivalent disruption, allowing a comparison of their SAC efficacy. B_3 oocytes treated with 25 nM nocodazole were compared with B_0 oocytes treated with varying doses of nocodazole 7 h after NEB (Fig. 5, A–C; and Fig. S2). We found that 35 nM nocodazole in B_0 oocytes gave the closest match to 25 nM in B_3 oocytes (Fig. 5, B and C). Under these conditions of matched bivalent disruption, we found that B_3 oocytes were more likely to arrest in MI (B_0, 6/36; B_3, 18/43; P = 0.026; Fig. 5 D). In those oocytes that did extrude polar bodies, there was no significant difference in the duration of MI (B_0, 10.5 ± 1.8, $n = 30$; B_3, 11.0 ± 1.6, $n = 25$; P = 0.3237; Fig. 5 E).

On examination of the securin destruction profiles in both B_0 and B_3 oocytes treated with nocodazole, it was apparent that there were two patterns of degradation (Fig. 5, F and G). First a typical profile, very similar to oocytes not treated with nocodazole, whereby securin is degraded continuously after APC activation, resulting in anaphase within a few hours (Fig. 5 G, blue trace). However, a second profile with transient switches from degradation to net synthesis of securin was commonly observed. We termed this event "stalling" and defined it as a period of at least 20 min during which degradation dropped to less than 15% per hour of securin (Fig. 5 G, green/red trace). This stalling event was equally common among B_0 and B_3 oocytes that arrested in MI but was significantly more common in B_3 oocytes than in B_0 in those oocytes that completed MI (MI arrest B_0, 3/6; MI arrest B_3, 10/18; P = 1; PBE B_0, 3/30; PBE B_3, 15/25; P = 0.0013; Fig. 5, H and I) and was associated only with oocytes treated with nocodazole, as it was never observed in untreated oocytes of any size (0/77 oocytes; not depicted).

We next used the securin traces to define the timing of APC activation and thus the length of prometaphase and metaphase, as we did for Fig. 2.

We found significant changes in these measures both between B_3 and B_0 oocytes with or without nocodazole, and

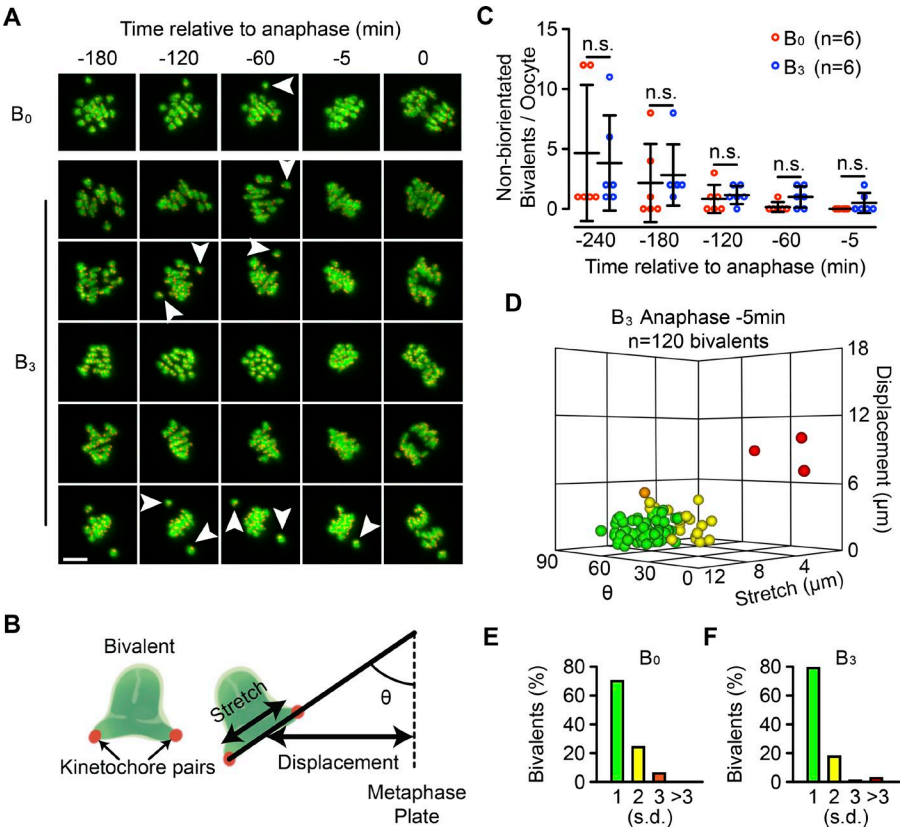

Figure 3. **Non-bioriented bivalents do not prevent APC activation in smaller oocytes.** (A) Representative time-lapse images of B_0 and B_3 oocytes expressing H2B-mCherry (green) and CenpC-GFP (red) with time relative to anaphase. Arrowheads indicate non-bioriented bivalents in both types of oocyte. Bar, 10 µm. (B) Cartoon depicting measurements of stretch, displacement and θ on a bivalent with sister kinetochore pairs (red). (C) Number of bivalents per oocyte classed as non-bioriented (>3 SDs from the control mean in any of the parameters of stretch, displacement, or θ) at times relative to anaphase; n.s. not significant. (D) 3D plot of bivalents in B_3 oocytes 5 min before anaphase, indicating the spread of stretch, displacement, and θ. Colors indicate the number of SDs a bivalent is, according to its worst-performing measure, from mean values defined by metaphase oocytes treated without nocodazole (green <1, yellow ≤2, orange ≤3, and red >3). (E and F) Proportion of bivalents falling within the stated number of SDs at anaphase −5 min for B_0 (E) and B_3 (F) oocytes. Error bars indicate SD.

also between those oocytes experiencing stalling and those not (Figs. 5 J and S3). Nocodazole addition resulted in modest increases in the duration of prometaphase and metaphase for both B_0 and B_3 oocytes when the nonstalled metaphase oocytes were considered. However, for both sizes of oocyte, stalling was associated with a much longer duration of MI, with increases predominantly in the time spent in metaphase (B_0 stalled, 6.5 ± 1.2, n = 3; B_0 nonstalled, 3.1 ± 1.3, n = 27; $P < 0.0001$; B_3 stalled, 4.7 ± 1.4, n = 10; B_3 nonstalled, 2.3 ± 0.7, n = 15; $P < 0.0001$). It is of note that in our experiment, only three B_0 oocytes experienced stalling; therefore, changes to the timing of MI in this group should be viewed with caution. A detailed analysis of statistical comparisons between all groups can be found in Fig. S3.

In summary, we find that when oocytes are exposed to doses of nocodazole designed to elicit a controlled disturbance to bivalent biorientation, the reduced size of the B_3 oocyte can temporarily stop the activity of the APC. This stalling of the APC was never seen in the absence of nocodazole and was rarely seen in full-size oocytes, suggesting that both the reduction in size and the additional stimulus of disrupted bivalents are required for an oocyte to inhibit the APC.

In summary, we have used a serial bisection technique to reduce the volume of mouse oocytes by more than 85%. It did not affect their ability to complete MI; however, it did result in a change in the size of the spindle, which reduced in proportion with oocyte volume, consistent with previous studies (Good et al., 2013; Hazel et al., 2013; Kyogoku and Kitajima, 2017). In small oocytes, we observed differences in APC timing (~1.4 h after securin degradation onset) and activity (~20% greater). One explanation of these findings is that an increased concentration of the kinetochore-derived SAC signal in a reduced volume causes greater control of the APC. This is consistent with the finding that the SAC strength grows as cells become smaller in the *C. elegans* embryo (Galli and Morgan, 2016) and that checkpoint function must depend on a balance between the relative SAC and APC strength (Wild et al., 2016). However, in small oocytes, as in full-sized oocytes, low doses of spindle poison generate large numbers of non-bioriented bivalents that do not prevent anaphase (Nagaoka et al., 2011; Gui and Homer, 2012; Kolano et al., 2012; Lane et al., 2012; Sebestova et al., 2012). Complete arrest in MI may not be expected, however, as even in mitotic cells, the SAC is not absolute in its ability to prevent anaphase and demonstrates a graded response proportional to the stimulus (Collin et al., 2013; Dick and Gerlich, 2013; Heinrich et al., 2013). An ~10-fold increase in the mean number of non-bioriented bivalents per small oocyte (5.4 vs. 0.5) caused only transient blocks to APC activity and thus did not prevent anaphase. We conclude that volume is not the only factor that uncouples chromosome biorientation from APC activity in oocytes.

Kyogoku and Kitajima (2017) have demonstrated that a robust checkpoint can be enforced only if oocyte volume is reduced before NEB. This enriches the mitotic checkpoint complex (MCC) in the half-oocyte containing the nucleus, because it is generated at nuclear pores (Rodriguez-Bravo et al., 2014; Kyogoku and Kitajima, 2017). In addition, other checkpoint kinases are known to have roles in G2 that influence SAC efficacy in mitosis (Yu et al., 2017) and so may also be enriched by halving before NEB. In our study, the reduction in volume was performed after NEB, and thus is more likely to reflect the ability of kinetochores to prevent anaphase with unperturbed concentrations of cytoplasmic APC inhibitors. In agreement with Kyogoku and Kitajima (2017), we find evidence that reduced volume can increase the ability of the SAC to control APC activ-

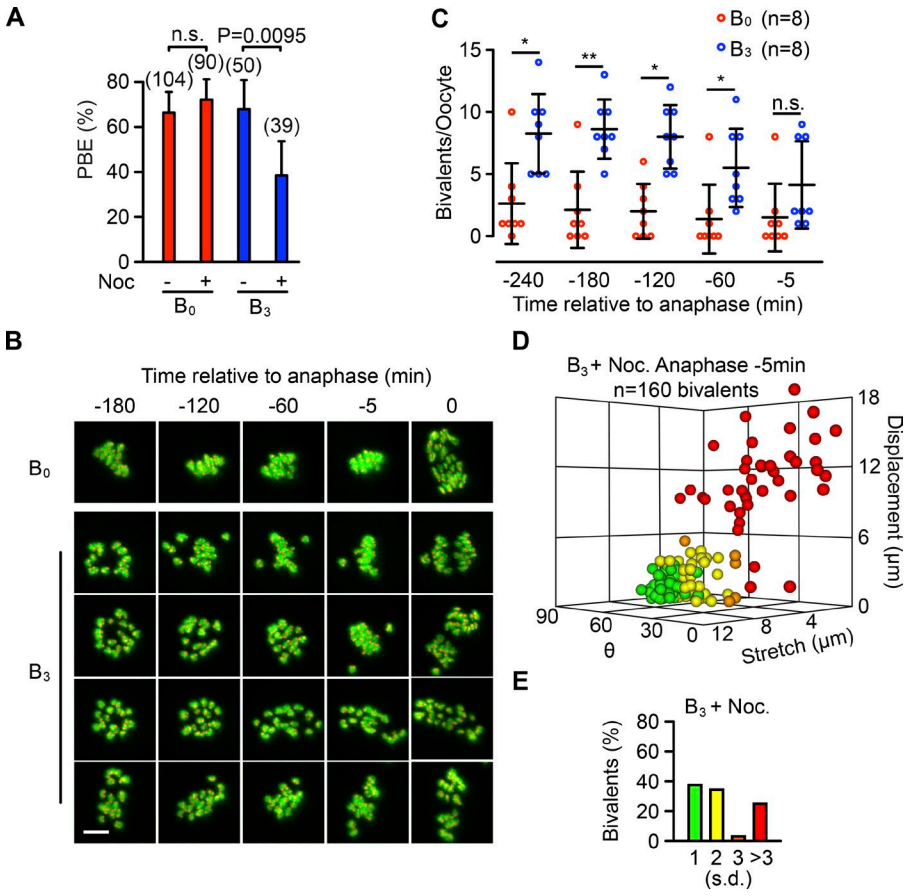

Figure 4. **Several non-bioriented bivalents fail to prevent APC activation in small oocytes.** (A) Percentage of B_0 and B_3 oocytes extruding polar bodies with or without addition of 25 nM nocodazole to the culture medium. Statistical test was Fisher's exact. Error bars indicate 95% confidence interval. (B) Representative time-lapse images of oocytes expressing H2B-mCherry and CenpC-GFP with time relative to anaphase. Bar, 10 µm. (C) Number of bivalents per oocyte classed as non-bioriented (>3 SDs from the control mean in any of the parameters of stretch, displacement, or θ) at times relative to anaphase. Statistical test is Dunn's multiple comparison test; n.s. not significant; *, $P < 0.05$; **, $P < 0.01$. (D) 3D scatterplot of bivalents 5 min before anaphase in B_3 oocytes cultured in 25 nM nocodazole. Colors indicate the number of SDs a bivalent is, according to its worst-performing measure, from mean values defined by metaphase oocytes treated without nocodazole (green <1, yellow ≤2, orange ≤3, and red >3). (E) Proportion of bivalents for B_0 oocytes falling within the stated number of SDs at anaphase −5 min.

ity, implying that size is a factor in explaining the weak spindle checkpoint of mammalian oocytes. However, by our method, the APC could not be inhibited sufficiently so as to prevent anaphase in response to non-bioriented bivalents, even when many persisted over long periods of time. Therefore, factors such as low levels of preformed MCC at NEB could play a role in the weakness of the SAC in oocytes.

Materials and methods

All reagents were from Sigma-Aldrich unless otherwise stated.

Animals and oocyte culture

4- to 6-wk-old C57BL/6 mice were used throughout. Oocytes were collected from mice 48–52 h after injection with 10 IU pregnant mare serum gonadotropin (Centaur Services) in M2 medium (Fulton and Whittingham, 1978) under mineral oil. 1 µM milrinone was added to maintain germinal vesicle stage arrest (Tsafriri et al., 1996). NEB in oocytes was synchronized by incubation in milrinone for 2 h, during which microinjections were performed if necessary. After washout of milrinone, the timing of NEB was recorded by eye at 10-min intervals. Oocytes not undergoing NEB within the modal time ±10 min were discarded from further study. Imaging and maturation studies were performed in M2 medium at 37°C.

cRNA manufacture

cRNA was transcribed in vitro from purified, linear dsDNA template using a mMessage T3 (H2B-mCherry, securin-YFP, and tubulin-GFP) or T7 (CenpC-GFP) RNA polymerase kit (Ambion) (Lane and Jones, 2014). cRNA was suspended in nuclease-free water, and its concentration was determined by photospectrometry.

Microinjection

cRNA microinjections were conducted in M2 medium covered in mineral oil on the stage of an inverted TE300 microscope (Nikon), using a 37°C heated chamber and micromanipulators (Narishige). cRNA was injected using timed pressure injections from a Picopump (World Precision Instruments) to achieve a size of 1–2% of the oocyte volume, with the following pipette tip cRNA concentrations: 500 ng/µl Securin; 250 ng/µl H2B; 600 ng/µl CenpC; and 500 ng/µl tubulin (gift from M.H. Verlhac, Collège de France, Paris, France; Holt et al., 2013; Levasseur, 2013).

Drug addition

Nocodazole at the final concentrations indicated (0–60 nM) was added to medium after completion of bisections and persisted throughout the remainder of the experiment. A stock concentration of 400 mM in DMSO was used, giving a final concentration of ≤0.015% DMSO. Partitioning of nocodazole into the mineral oil was minimized using glass bottomed 96-well imaging plates (MatTek) with 200 µl M2 medium capped with a minimal volume of mineral oil.

Confocal imaging and chromosome tracking

After bisections, oocytes injected with H2B-mCherry and either EGFP-CenpC or securin-YFP cRNA were placed on the stage of a Leica SP8 confocal microscope equipped with an environmental chamber at 37°C in M2 medium covered by mineral oil. Up to 20 3D images (17 *z*-sections, 320 × 320 pixels with 2.2-µm spacing; 32.3 × 32.3 × 35.2 µm) were acquired every 300 s using a 40× ob-

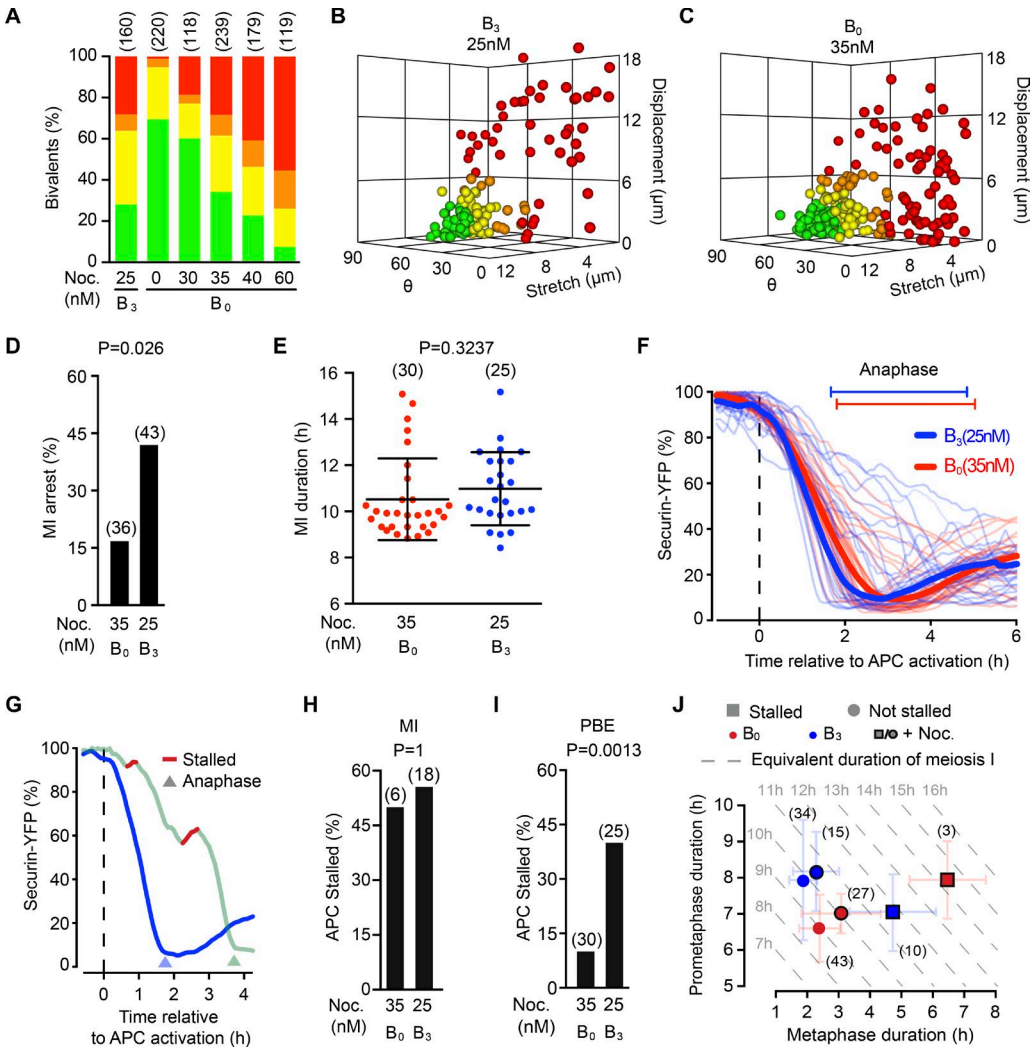

Figure 5. **Matched doses of nocodazole reveal differences in APC activity with reduced oocyte volume.** (A) B_0 oocytes were matured in the indicated concentrations of nocodazole and assessed for bivalent biorientation 6 h after NEB. Colors indicate the number of SDs a bivalent is, according to its worst-performing measure, from mean values defined by metaphase oocytes treated without nocodazole (green <1, yellow ≤2, orange ≤3, and red >3). (B and C) 3D scatterplots showing the extent of chromosome biorientation in B_3 oocytes (25 nM nocodazole; B) and B_0 oocytes (35 nM nocodazole; C) as in A. (D) Percentage of oocytes of the indicated size extruding polar bodies after 15-h culture in the indicated concentration of nocodazole. (E) Duration of MI, defined as the time from NEB to anaphase. (F) Individual (pale) and mean (bold) securin traces from B_0 and B_3 oocytes, arranged relative to the time of APC activation. Horizontal bars show the corresponding timing of anaphase. (G) Representative traces of two modes of securin degradation found in B_3 oocytes matured in 25 nM nocodazole. Arrowheads indicate the timing of anaphase. Red color indicates periods of stalling. (H) Proportion of MI-arrested oocytes that exhibited stalling. (I) Proportion of oocytes that completed MI that exhibited stalling. (J) Results from experiments with and without nocodazole addition are presented together for comparison of the effects of oocyte volume reduction and addition of matched doses of nocodazole. Blue points, B_3 oocytes; red, B_0; round points, no stalling event was detected; square points, stalling. Back border indicates the presence of nocodazole (25 nM for B_3 and 35 nM for B_0). Parentheses indicate number of oocytes. Error bars are SDs. Gray dashed lines indicate points where the duration of MI (prometaphase + metaphase) is the same. Statistical comparisons between all points are indicated in Fig. S3. In A, D, E, and G–I, numbers of oocytes are indicated in parenthesis. Statistical tests used were Fisher's exact test (D, H, and I) and unpaired *t* test (E).

jective (NA 1.3, oil immersion) and 9× zoom. Chromosome tracking by in-laboratory software (Python) that controlled the microscope via communication with the SP8's Matrix Screener module ensured that the chromosomes remained in the center of the imaging volume throughout maturation (Lane et al., 2017). Securin-YFP and difference interference contrast images were also acquired every 300 s, but with 0.75× zoom.

Image processing

Images from chromosome tracking experiments were processed using ImageJ macros by subtraction of a 2-pixel Gaussian blur from a 10-pixel Gaussian blur background as described (Kitajima et al., 2011).

Oocyte bisection

After washout of milrinone, but before NEB, oocytes were prepared by removal of the zona pellucida using a brief incubation (~5 s with pipetting) in acid Tyrode's solution followed by three washes to remove traces of acid. Oocytes were then incubated in 2 mM cytochalasin D until NEB occurred. Bisections were performed immediately after NEB on 1% agar gels made with PBS and equilibrated with M2 medium containing ~2 µM cytochalasin D. Oocytes were either bisected up to three times, resulting in one-half, one-quarter, or one-eighth parts, or sham bisected three times by leaving a narrow cytoplasmic bridge that allowed the two halves to regroup (Fig. 1 A). Bisection was performed manually under a stereomicroscope with a heated stage (37°C) using a fine fiber drawn from a glass pipette in a flame.

Chromosome counting

B_3 oocytes injected with H2B-mCherry and CenpC-GFP were imaged by confocal microscope with 1-µm *z*-sections during prometaphase (before chromosome congression on the spindle). Chromosomes were counted by labeling each kinetochore pair in the 3D stack using laboratory-made ImageJ macros.

Chromosome biorientation analysis

Analysis of bivalent biorientation was done by registering kinetochore positions in 3D confocal stacks using in-laboratory ImageJ macros. Macros label kinetochores non-permanently in the images to prevent users from registering the same kinetochore twice and to allow the kinetochores belonging to the same bivalent to be registered in pairs. Using the kinetochore position data, a subsequent macro implements a best-fit algorithm to determine the position and normal angle of the spindle equator. The position and direction of the spindle equator is then used to calculate the displacement from, and angle of intersection with, each bivalent, giving measures of displacement and θ, respectively. Interkinetochore distance, or stretch, is calculated as the 3D distance between the two kinetochores of each bivalent. Control oocytes matured to metaphase (NEB + 8 h) were used to create a dataset. The mean and SD for bivalent stretch, displacement, and angle of bivalents in this group were used to define a standard metaphase. Each bivalent in the experimental groups was compared with this standard. The number of SDs away from the control mean was calculated for stretch, displacement, and angle, and the worst-performing metric was used to color that bivalent. Colors were assigned as follows: if the worst metric is <1 SD from the mean, it is colored green; ≥1 SD and <2 SD, yellow; ≥2 SD and <3 SD, orange; and ≥3 SD, red. So a bivalent with stretch and displacement within 1 SD of their respective control means, but with angle greater than 1 SD and less than 2 SD from the control mean, would be colored yellow (<2 SD from the mean). These are the colors used in the scatterplots in Figs. 3, 4, 5, and S2.

Volume calculations

Oocyte volume was calculated by measuring the diameter of the oocyte twice in a 2D image (height and width), then calculating the radius from the mean. Radius (micrometers) was converted to volume (picoliter) volume using the formula $V = 4/3000 \times \pi \times r^3$. Spindle volume was calculated as $V = 4/3000 \times \pi \times 0.5L \times 0.5W^2$, where L is the long axis and W the short axis of the spindle.

Data analysis

Fluorescence intensities were recorded from regions of interest encompassing the oocytes using ImageJ and stored in Microsoft Excel spreadsheets. Fluorescence traces were background-subtracted and normalized with maxima at 100%.

APC activity

Empirical securin-YFP degradation data were imported into Matlab (R2013a; MathWorks). The timing of securin degradation onset (APC activation) was determined such that time point *t* was the first time point at which there was a significant difference between the previous and the subsequent 15 readings. Curve fitting (Fourier 3) was used to fit the data in the region of securin degradation, and the first differential of this was used to calculate the maximal rate of securin-YFP degradation achieved.

Statistical analysis

Statistical analysis was performed using Prism (GraphPad Software). Analysis of variance was used with Tukey's multiple comparison test for normally distributed data or Dunn's multiple comparison test for nonparametric data.

Online supplemental material

Fig. S1 shows that the bisection procedure did not cause loss of bivalents, nor did it prevent formation of spindles with normal proportions. Fig. S2 shows the bivalent biorientation results for B_0 oocytes treated with various doses of nocodazole, to establish a dose matching B_3 biorientation in 25 nM nocodazole. Fig. S3 shows the duration of MI and the lengths of prometaphase and metaphase for B_0 and B_3 oocytes treated with or without nocodazole (related to Fig. 5 J) and provides a summary of statistically significant differences. Videos 1 and 2 show time lapses of B_3 oocytes with labeled chromosomes and kinetochores during MI with and without 25 nM nocodazole, respectively.

Acknowledgments

We thank Dr. Marie Hélène Verlhac for the gift of tubulin-GFP.

This work was funded by a project grant to K.T. Jones from the Australian Research Council (DP120100946).

The authors declare no competing financial interests.

Author contributions: S.I.R. Lane conceived the study, designed and performed the experiments, and analyzed the data. S.I.R. Lane and K.T. Jones wrote the manuscript.

Submitted: 30 June 2016
Revised: 28 July 2017
Accepted: 7 September 2017

References

Clute, P., and Y. Masui. 1995. Regulation of the appearance of division asynchrony and microtubule-dependent chromosome cycles in Xenopus laevis embryos. *Dev. Biol.* 171:273–285. https://doi.org/10.1006/dbio.1995.1280

Clute, P., and J. Pines. 1999. Temporal and spatial control of cyclin B1 destruction in metaphase. *Nat. Cell Biol.* 1:82–87. https://doi.org/10.1038/10049

Collin, P., O. Nashchekina, R. Walker, and J. Pines. 2013. The spindle assembly checkpoint works like a rheostat rather than a toggle switch. *Nat. Cell Biol.* 15:1378–1385. https://doi.org/10.1038/ncb2855

Collins, J.K., S.I.R. Lane, J.A. Merriman, and K.T. Jones. 2015. DNA damage induces a meiotic arrest in mouse oocytes mediated by the spindle assembly checkpoint. *Nat. Commun.* 6:8553. https://doi.org/10.1038/ncomms9553

Dick, A.E., and D.W. Gerlich. 2013. Kinetic framework of spindle assembly checkpoint signalling. *Nat. Cell Biol.* 15:1370–1377. https://doi.org/10.1038/ncb2842

Foley, E.A., and T.M. Kapoor. 2013. Microtubule attachment and spindle assembly checkpoint signalling at the kinetochore. *Nat. Rev. Mol. Cell Biol.* 14:25–37. https://doi.org/10.1038/nrm3494

Fulton, B.P., and D.G. Whittingham. 1978. Activation of mammalian oocytes by intracellular injection of calcium. *Nature.* 273:149–151. https://doi.org/10.1038/273149a0

Galli, M., and D.O. Morgan. 2016. Cell size determines the strength of the spindle assembly checkpoint during embryonic development. *Dev. Cell.* 36:344–352. https://doi.org/10.1016/j.devcel.2016.01.003

Good, M.C., M.D. Vahey, A. Skandarajah, D.A. Fletcher, and R. Heald. 2013. Cytoplasmic volume modulates spindle size during embryogenesis. *Science.* 342:856–860. https://doi.org/10.1126/science.1243147

Gorbsky, G.J. 2015. The spindle checkpoint and chromosome segregation in meiosis. *FEBS J.* 282:2471–2487. https://doi.org/10.1111/febs.13166

Gui, L., and H. Homer. 2012. Spindle assembly checkpoint signalling is uncoupled from chromosomal position in mouse oocytes. *Development.* 139:1941–1946. https://doi.org/10.1242/dev.078352

Hached, K., S.Z. Xie, E. Buffin, D. Cladière, C. Rachez, M. Sacras, P.K. Sorger, and K. Wassmann. 2011. Mps1 at kinetochores is essential for female mouse meiosis I. *Development.* 138:2261–2271. https://doi.org/10.1242/dev.061317

Hazel, J., K. Krutkramelis, P. Mooney, M. Tomschik, K. Gerow, J. Oakey, and J.C. Gatlin. 2013. Changes in cytoplasmic volume are sufficient to drive spindle scaling. *Science.* 342:853–856. https://doi.org/10.1126/science.1243110

Heasley, L.R., S.M. Markus, and J.G. DeLuca. 2017. "Wait anaphase" signals are not confined to the mitotic spindle. *Mol. Biol. Cell.* 28:1186–1194. https://doi.org/10.1091/mbc.E17-01-0036

Heinrich, S., E.-M. Geissen, J. Kamenz, S. Trautmann, C. Widmer, P. Drewe, M. Knop, N. Radde, J. Hasenauer, and S. Hauf. 2013. Determinants of robustness in spindle assembly checkpoint signalling. *Nat. Cell Biol.* 15:1328–1339. https://doi.org/10.1038/ncb2864

Herbert, M., M. Levasseur, H. Homer, K. Yallop, A. Murdoch, and A. McDougall. 2003. Homologue disjunction in mouse oocytes requires proteolysis of securin and cyclin B1. *Nat. Cell Biol.* 5:1023–1025. https://doi.org/10.1038/ncb1062

Hoffmann, S., B. Maro, J.Z. Kubiak, and Z. Polanski. 2011. A single bivalent efficiently inhibits cyclin B1 degradation and polar body extrusion in mouse oocytes indicating robust SAC during female meiosis I. *PLoS One.* 6:e27143. https://doi.org/10.1371/journal.pone.0027143

Holt, J.E., S.I.R. Lane, and K.T. Jones. 2013. Time-lapse epifluorescence imaging of expressed cRNA to cyclin B1 for studying meiosis I in mouse oocytes. *Methods Mol. Biol.* 957:91–106. https://doi.org/10.1007/978-1-62703-191-2_6

Homer, H.A., A. McDougall, M. Levasseur, K. Yallop, A.P. Murdoch, and M. Herbert. 2005. Mad2 prevents aneuploidy and premature proteolysis of cyclin B and securin during meiosis I in mouse oocytes. *Genes Dev.* 19:202–207. https://doi.org/10.1101/gad.328105

Jia, L., S. Kim, and H. Yu. 2013. Tracking spindle checkpoint signals from kinetochores to APC/C. *Trends Biochem. Sci.* 38:302–311. https://doi.org/10.1016/j.tibs.2013.03.004

Jones, K.T., and S.I.R. Lane. 2013. Molecular causes of aneuploidy in mammalian eggs. *Development.* 140:3719–3730. https://doi.org/10.1242/dev.090589

Kitajima, T.S., M. Ohsugi, and J. Ellenberg. 2011. Complete kinetochore tracking reveals error-prone homologous chromosome biorientation in mammalian oocytes. *Cell.* 146:568–581. https://doi.org/10.1016/j.cell.2011.07.031

Kolano, A., S. Brunet, A.D. Silk, D.W. Cleveland, and M.-H. Verlhac. 2012. Error-prone mammalian female meiosis from silencing the spindle assembly checkpoint without normal interkinetochore tension. *Proc. Natl. Acad. Sci. USA.* 109:E1858–E1867. https://doi.org/10.1073/pnas.1204686109

Kyogoku, H., and T.S. Kitajima. 2017. Large cytoplasm is linked to the error-prone nature of oocytes. *Dev. Cell.* 41:287–298.e4. https://doi.org/10.1016/j.devcel.2017.04.009

Lane, S.I., and K.T. Jones. 2014. Non-canonical function of spindle assembly checkpoint proteins after APC activation reduces aneuploidy in mouse oocytes. *Nat. Commun.* 5:3444. https://doi.org/10.1038/ncomms4444

Lane, S.I.R., Y. Yun, and K.T. Jones. 2012. Timing of anaphase-promoting complex activation in mouse oocytes is predicted by microtubule-kinetochore attachment but not by bivalent alignment or tension. *Development.* 139:1947–1955. https://doi.org/10.1242/dev.077040

Lane, S.I.R., S. Crouch, and K.T. Jones. 2017. Imaging chromosome separation in mouse oocytes by responsive 3D confocal timelapse microscopy. *Methods Mol. Biol.* 1471:245–254

Levasseur, M. 2013. Making cRNA for microinjection and expression of fluorescently tagged proteins for live-cell imaging in oocytes. *Methods Mol. Biol.* 957:121–134. https://doi.org/10.1007/978-1-62703-191-2_8

Liu, D., H. Shao, H. Wang, and X.J.J. Liu. 2014. Meiosis I in Xenopus oocytes is not error-prone despite lacking spindle assembly checkpoint. *Cell Cycle.* 13:1602–1606. https://doi.org/10.4161/cc.28562

McGuinness, B.E., M. Anger, A. Kouznetsova, A.M. Gil-Bernabé, W. Helmhart, N.R. Kudo, A. Wuensche, S. Taylor, C. Hoog, B. Novak, and K. Nasmyth. 2009. Regulation of APC/C activity in oocytes by a Bub1-dependent spindle assembly checkpoint. *Curr. Biol.* 19:369–380. https://doi.org/10.1016/j.cub.2009.01.064

Merriman, J.A., S.I. Lane, J.E. Holt, P.C. Jennings, I. García-Higuera, S. Moreno, E.A. McLaughlin, and K.T. Jones. 2013. Reduced chromosome cohesion measured by interkinetochore distance is associated with aneuploidy even in oocytes from young mice. *Biol. Reprod.* 88:31. https://doi.org/10.1095/biolreprod.112.104786

Minshull, J., H. Sun, N.K. Tonks, and A.W. Murray. 1994. A MAP kinase-dependent spindle assembly checkpoint in Xenopus egg extracts. *Cell.* 79:475–486.

Musacchio, A. 2015. The molecular biology of spindle assembly checkpoint signaling dynamics. *Curr. Biol.* 25:R1002–R1018. https://doi.org/10.1016/j.cub.2015.08.051

Nagaoka, S.I., C.A. Hodges, D.F. Albertini, and P.A. Hunt. 2011. Oocyte-specific differences in cell-cycle control create an innate susceptibility to meiotic errors. *Curr. Biol.* 21:651–657. https://doi.org/10.1016/j.cub.2011.03.003

Pesenti, M.E., J.R. Weir, and A. Musacchio. 2016. Progress in the structural and functional characterization of kinetochores. *Curr. Opin. Struct. Biol.* 37:152–163. https://doi.org/10.1016/j.sbi.2016.03.003

Polanski, Z., and J.Z. Kubiak. 2013. Free-hand bisection of mouse oocytes and embryos. *Methods Mol. Biol.* 957:255–265. https://doi.org/10.1007/978-1-62703-191-2_18

Rieder, C.L., A. Khodjakov, L.V. Paliulis, T.M. Fortier, R.W. Cole, and G. Sluder. 1997. Mitosis in vertebrate somatic cells with two spindles: Implications for the metaphase/anaphase transition checkpoint and cleavage. *Proc. Natl. Acad. Sci. USA.* 94:5107–5112. https://doi.org/10.1073/pnas.94.10.5107

Rodriguez-Bravo, V., J. Maciejowski, J. Corona, H.K. Buch, P. Collin, M.T. Kanemaki, J.V. Shah, and P.V. Jallepalli. 2014. Nuclear pores protect genome integrity by assembling a premitotic and Mad1-dependent anaphase inhibitor. *Cell.* 156:1017–1031. https://doi.org/10.1016/j.cell.2014.01.010

Schuh, M., and J. Ellenberg. 2007. Self-organization of MTOCs replaces centrosome function during acentrosomal spindle assembly in live mouse oocytes. *Cell.* 130:484–498. https://doi.org/10.1016/j.cell.2007.06.025

Sebestova, J., A. Danylevska, L. Novakova, M. Kubelka, and M. Anger. 2012. Lack of response to unaligned chromosomes in mammalian female gametes. *Cell Cycle.* 11:3011–3018.

Shao, H., R. Li, C. Ma, E. Chen, and X.J. Liu. 2013. *Xenopus* oocyte meiosis lacks spindle assembly checkpoint control. *J. Cell Biol.* 201:191–200.

Touati, S.A., and K. Wassmann. 2016. How oocytes try to get it right: spindle checkpoint control in meiosis. *Chromosoma.* 125:321–335.

Tsafriri, A., S.Y. Chun, R. Zhang, A.J. Hsueh, and M. Conti. 1996. Oocyte maturation involves compartmentalization and opposing changes of cAMP levels in follicular somatic and germ cells: studies using selective phosphodiesterase inhibitors. *Dev. Biol.* 178:393–402. https://doi.org/10.1006/dbio.1996.0226

Wild, T., M.S.Y. Larsen, T. Narita, J. Schou, J. Nilsson, and C. Choudhary. 2016. The spindle assembly checkpoint is not essential for viability of human cells with genetically lowered APC/C activity. *Cell Reports.* 14:1829–1840. https://doi.org/10.1016/j.celrep.2016.01.060

Yu, F., Y. Jiang, L. Lu, M. Cao, Y. Qiao, X. Liu, D. Liu, T. Van Dyke, F. Wang, X. Yao, et al. 2017. Aurora-A promotes the establishment of spindle assembly checkpoint by priming the Haspin-Aurora-B feedback loop in late G2 phase. *Cell Discov.* 3:16049. https://doi.org/10.1038/celldisc.2016.49

Zhang, M., P. Kothari, and M.A. Lampson. 2015. Spindle assembly checkpoint acquisition at the mid-blastula transition. *PLoS One.* 10:e0119285. https://doi.org/10.1371/journal.pone.0119285